Experimental and numerical investigation of the behaviour of complex shaped particles in a model scale fluidized bed

K. VOLLMARI[1] AND H. KRUGGEL-EMDEN[1]

[1]Ruhr-University Bochum
Universitätsstr. 150, IC 2/107
Vollmari@leat.rub.de, http://www.leat.ruhr-uni-bochum.de/

Key words: DEM, CFD, Experiments, Complex Shaped Particles, Fluidization, Orientations.

Abstract. *In this study a laboratory scale fluidized bed is examined experimentally and numerically through a coupled discrete element method (DEM) and computational fluid dynamics (CFD) approach. Five differently shaped Geldart D particle groups including spheres, cylinders and cuboids are considered. Numerically obtained results for the pressure drop are in good agreement with experiments for most particles. A study on particle orientations is performed which gives valuable insight into deviations between experiments and simulations. The DEM-CFD correctly describes preferred orientations taken up by elongated particles in the fluid flow.*

1 INTRODUCTION

Fluidized beds are widely used in process and energy engineering as they possess favourable characteristics such as fast mixing, uniform temperature distribution and high gas-solid contact. The pressure drop is a key parameter for the characterization of a fluidized bed and is subject to fluctuations. Besides experiments and correlations simulations can be used for the prediction of the pressure drop. With growing computational power numerical simulations with a coupled discrete element method (DEM) and computational fluid dynamics (CFD) approach recently became feasible for the simulation of fluidized systems. Previously most simulations were conducted with spherical particles only, which cannot precisely predict the behavior of real, complex shaped particles like encountered in biomass. With the introduction of new submodels [1, 2] to the DEM-CFD which consider the particle shape and orientation it has become possible to simulate fluidized beds with complex shaped particles [3–5]. As there is an ongoing discussion about the validity of certain submodels, experimental validation is necessary. In this study pressure drops and particle orientations for five differently shaped Geldart D particle groups, including spheres, cylinders and cuboids are experimentally and numerically examined.

2 METHODOLOGY

In the coupled DEM-CFD particles are tracked discretely while the fluid phase is represented through a cell-averaged continuum. In the discrete element method the translational and rotational particle motion is obtained by integrating Newton's and Euler's equations

$$m_i \frac{d^2\vec{x}_i}{dt^2} = \vec{F}_i^c + \vec{F}_i^{pf} + m_i\vec{g}, \tag{1}$$

$$\hat{I}_i \frac{d\vec{W}_i}{dt} + \vec{W}_i \times \left(\hat{I}_i\vec{W}_i\right) = \Lambda_i^{-1}\vec{M}_i, \tag{2}$$

with the particle mass m_i, particle acceleration $d^2\vec{x}_i/dt^2$, contact force $\vec{F}_i^c$, particle/fluid force $\vec{F}_i^{pf}$, gravitational force $m_i\vec{g}$, angular acceleration $d\vec{W}_i/dt$, angular velocity $\vec{W}_i$, external moment resulting out of contact or particle/fluid forces $\vec{M}_i$, the inertia tensor along the principal axis $\hat{I}_i$ and the rotation matrix converting a vector from the inertial into the body fixed frame Λ_i^{-1}.

Contact force laws are applied similarly as used for spherical particles [6, 7]. A linear spring damper model is used to provide the normal component of the contact forces

$$\vec{F}^n = k^n\delta\vec{n} + \gamma^n\vec{v}_{rel}^n, \tag{3}$$

where k^n is the spring stiffness, δ the virtual overlap, $\vec{n}$ a normal vector, γ^n a damping coefficient and $\vec{v}_{rel}^n$ the normal velocity in the contact point. Both k^n and γ^n determine the coefficient of normal restitution between particles e_{PP}^n as well as particles and walls e_{PW}^n. For the calculation of the tangential forces a linear spring limited by the Coulomb condition is used

$$\vec{F}^t = -min\left(k^t\left|\vec{\xi}\right|, \mu_C\left|\vec{F}^n\right|\right)\cdot\vec{t}, \tag{4}$$

where k^t is the stiffness of a linear spring, μ_C is the friction coefficient, $\vec{\xi}$ is the relative tangential displacement and $\vec{t}$ is the tangential unit vector. No rotational friction is considered.

Computational Fluid Dynamics (CFD) in an Eulerian framework is used to describe the fluid phase. The fluid velocity is addressed as a spatially averaged quantity in each cell of a Cartesian grid. The equation of continuity (5) and the equation of momentum (6) are solved

$$\frac{\partial(\varepsilon_f\rho_f)}{\partial t} + \nabla\left(\varepsilon_f\rho_f\vec{u}\right) = 0, \tag{5}$$

$$\frac{\partial(\varepsilon_f\rho_f\vec{u})}{\partial t} + \nabla\left(\varepsilon_f\rho_f\vec{u}\vec{u}\right) = -\varepsilon_f\nabla\mathrm{p} + \nabla\left(\overline{\overline{\varepsilon_f\tau}}\right) + \varepsilon_f\rho_f\vec{g} + \vec{f}_{int}, \tag{6}$$

where $\vec{u}_f$, ρ_f and p are the physical fluid velocity, density and pressure. $\vec{f}_{int}$ is the volumetric particle/fluid interaction applied in each CFD cell, ε_f is the local fluid porosity and $\bar{\bar{\tau}}$ is the fluid viscous stress tensor $\bar{\bar{\tau}} = \eta_\mathrm{e}\left[\left(\nabla\vec{u}_f\right) + \left(\nabla\vec{u}_f\right)^{-1}\right]$ with η_e the effective viscosity determined from the standard k-ε turbulent model. The particle/fluid interaction $\vec{f}_{int}$ is given component wise as $f_{int_i} = \bar{\beta}_i(u_i - \bar{v}_i)$, where $\bar{v}_i$ is the fluid cell averaged particle velocity and $\bar{\beta}_i$ is the fluid cell averaged particle/fluid friction coefficient with *i=x, y, z*.

The particle/fluid force $\vec{F}_i^{pf}$ consists of all individual particle/fluid forces including the drag force $\vec{F}_i^d$ and pressure gradient force $\vec{F}_i^{\nabla p}$ acting on a particle *i* written as $\vec{F}_i^{pf} = \vec{F}_i^d + \vec{F}_i^{\nabla p}$. The approach by Di Felice [1], where the force for an isolated spherical particle is calculated and altered by the influence of surrounding particles is also suitable for non-spherical particles. The respective force reads

$$\vec{F}_i^{pf} = \vec{F}_i^{d} + \vec{F}_i^{\nabla p} = \frac{1}{2}\rho_f \left|\vec{u}_f - \vec{v}_i\right| C_D A_\perp {\varepsilon_f}^{1-\chi}\left(\vec{u}_f - \vec{v}_i\right) \tag{7}$$

where C_D is the drag coefficient, $A_\perp$ is the cross-sectional area perpendicular to the flow and χ a correction factor. Equation (7) can be rewritten in terms of the particle/fluid friction coefficient as

$$\vec{\beta}_i = \frac{1}{2}\rho_f C_D A_\perp \varepsilon_f \left|\vec{u}_f - \vec{v}_i\right| \left(1-\varepsilon_f\right) \frac{1}{V_i} {\varepsilon_f}^{(1-\chi)}. \tag{8}$$

with $\chi = 3.7 - 0.65\exp(-(1.5-\log(Re))^2/2)$ as a function of the particle Reynolds-number $Re = \varepsilon_f \rho_f d_e \left|\vec{u}_f - \vec{v}_i\right| / \eta_\mathrm{f}$. Here d_e describes the diameter of a volume equivalent spherical particle and η_f the fluid viscosity. The drag coefficient C_D of a single particle (including complex shapes) can be derived from correlations such as Hölzer und Sommerfeld [2] which can be written as

$$C_D = \frac{8}{Re}\frac{1}{\sqrt{\phi_\perp}} + \frac{16}{Re}\frac{1}{\sqrt{\phi}} + \frac{3}{\sqrt{Re}}\frac{1}{\phi^{3/4}} + 0.42\times 10^{0.4(-\log(\phi))^{0.2}}\frac{1}{\phi_\perp} \tag{9}$$

where $\phi_\perp$ is the crosswise sphericity which is the ratio between the cross-sectional area of the volume equivalent sphere and the projected cross-sectional area of the considered particle perpendicular to the flow.

3 EXPERIMENTAL AND NUMERICAL SETUP

To carry out the experiments a laboratory scale fluidized bed made from antistatic polycarbonate with the dimensions width = depth = 0.11 m and height = 0.41 m, displayed in Fig. 1 was used. The solid matter is placed on a porous plate with an open area of 37%. A pressure tapping point slightly below the porous plate and one in the vessel at h=31 cm are used to measure the differential pressure with a pressure transducer of the type Newport Omega PD41X-V-50 mbar. Images of the experiment were taken with a high speed camera (Optronis CL600x2) at 25 frames per second over a time period of 15 seconds. Geldart-D type beech wood particles including spherical, cylindrical or cuboidal shapes are used, see Table 1.

Table 1 Particle properties including the particle dimensions, the sphericity ϕ, the particle density ρ_p, the initial bed height L_{fb} and the averaged porosity $\bar{\varepsilon}$ of the fixed bed

Shape	Sphere	Ideal Cylinder	Cube	Elongated Cylinder	Elongated Cuboid
	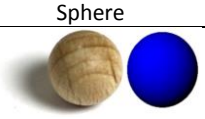		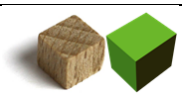		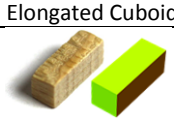
Size [mm]	7.2	6.1 6.2	5.2 6.3 6.3	3.9 14.0	4.2 4.2 11.4
ϕ [-]	1.00	0.87	0.80	0.75	0.73
ρ_p [kg/m³]	772.5	708.5	746.9	764.4	639.7
L_{fb} [mm] /$\bar{\varepsilon}$ [-]	95 0.40	98 0.36	103 0.43	103 0.44	115 0.40

The combination of beech wood and the antistatic polycarbonate of the vessel ensures that no electrostatic effects disturb the experiments. Attrition or breakage do not occur.

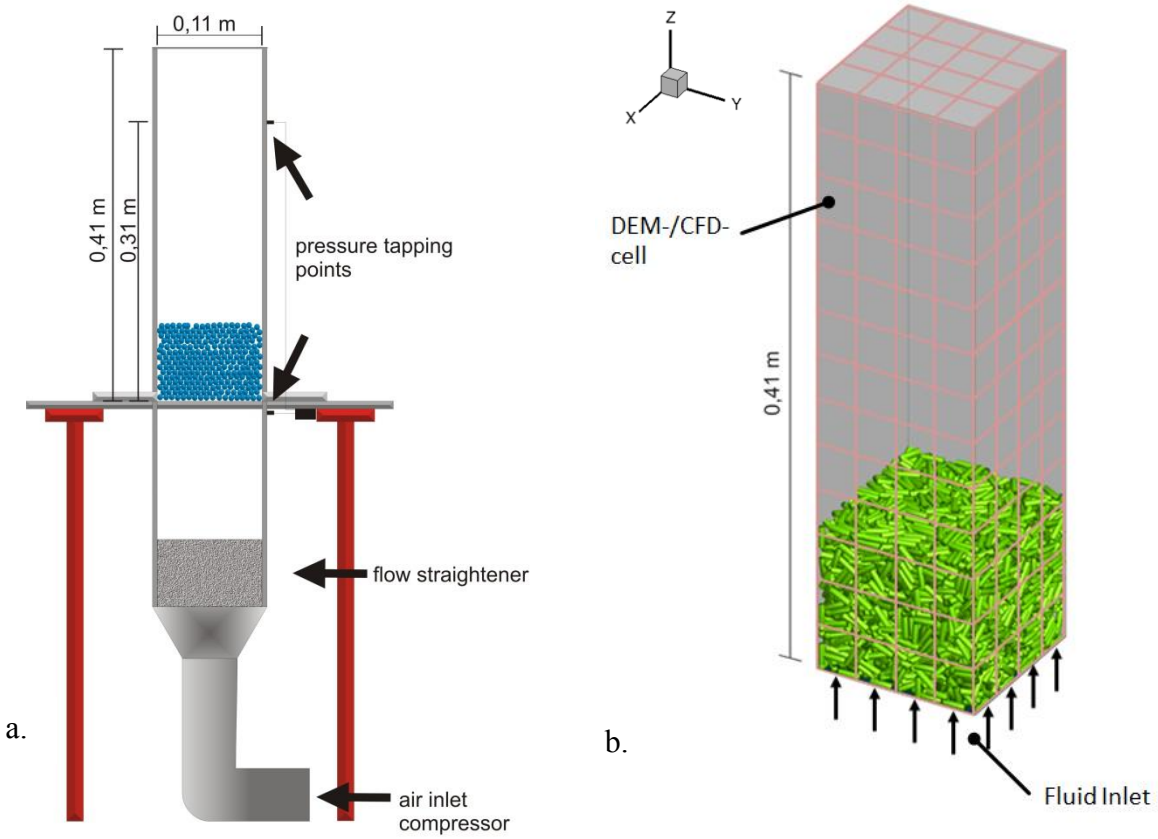

Fig. 1 Experimental (a) and numerical (b) setup and its division into a number of DEM-CFD cells larger than the particle size

The particle mass was kept constant for all experiments at m= 0.535 kg. The superficial velocity has been increased in steps of 0.1 m/s starting at 0.4 m/s up to 2.4 m/s for all particles. The numerical setup was chosen so that all dimensions and operation conditions remain equal. Cylindrical and cuboidal particles are represented through a polyhedron approximation [8]. The friction and restitution coefficients were determined according to procedures described by Höhner et al. [9] and Hold [10] on the single particle level, respectively.

4 RESULTS AND DISCUSSION

4.1 Pressure drop analysis

Mean pressure drops in experiments and corresponding coupled DEM-CFD simulations are outlined for 5 different particle shapes in Fig. 2. Multiple repetitions have been performed for the experiments and simulations; the error bars show the obtained variations in terms of minimal and maximal values.

Fig. 2a shows the results for d=7 mm spherical particles. Good agreement between simulation and experiment can be observed. For velocities U < 1.4 m/s there is a mean deviation of $\overline{\Delta p} = 23\ Pa$, for the fluidized range from U > 1.4 m/s onwards an average deviation of

$\overline{\Delta p} = 8\,Pa$ is obtained. Results for ideal cylinders with the dimensions 6 mm x 6 mm are given in Fig. 2b. Good agreement between experiment and simulation can be seen over the entire velocity range, especially in the fixed bed regime with an average pressure drop difference of only $\overline{\Delta p} = 15\,Pa$.

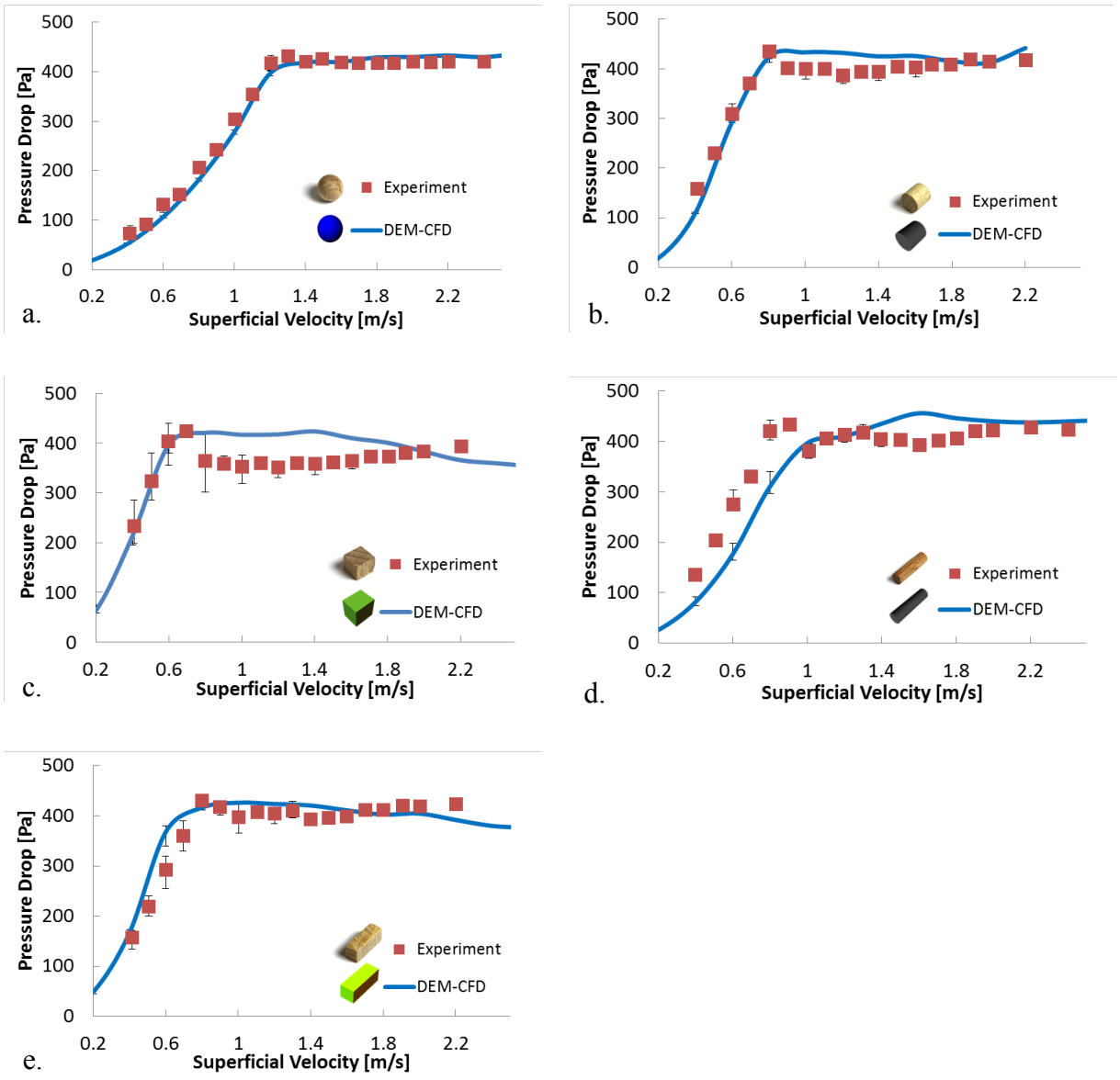

Fig. 2 Pressure drops of five differently shaped particle groups obtained for increasing superficial gas velocities in simulations and experiments for (a) 7 mm spheres, (b) 6 mm x 6 mm ideal cylinders, (c) 5 mm x 6 mm x 6 mm cubes, (d) 4 mm x 14 mm elongated cylinders and (e) 4 mm x 4 mm x 11 mm cuboids

Results for 5 mm x 6 mm x 6 mm cubes are displayed in Fig. 2c. High variations between the minimum and maximum values can be observed in the fixed bed range of the experiments,

nonetheless the simulation is in good agreement with the experimental average value. Different initial bed structures with locally deviating porosities are the reason for the scatter of the experimental values. Opposite to spheres and cylinders, the porosity in packings of cubes can reach values of nearly 0 if the particles align themselves with each other. The deviation of the pressure drop between simulation and experiment increases once the minimum fluidization velocity is passed at $U_{mf} > 0.7$ m/s with $\overline{\Delta p} = 44\ Pa$. This is the result of an incomplete fluidization in the experiment, as stacks of particles are not in motion in the corners of the vessel. The same occurs in the simulation at higher velocities, so that the pressure drop declines starting at U= 1.4 m/s.

Results for elongated cylinders with the dimensions 4 mm x 14 mm are displayed in Fig. 2d. A deviation between experiment and simulation of $\overline{\Delta p} = 120\ Pa$ can be observed for the fixed bed regime at $U_{mf} < 0.9$ m/s. Particle shapes that differ strongly from that of a sphere show the tendency to form channels at low superficial velocities, which is the case for 4 mm x 14 mm cylinders for superficial velocities between 0.9 m/s < U < 1.6 m/s. The simulation does not reproduce this behavior, as the fluid velocity is only represented through an averaged grid based velocity. Therefore the differences in the velocities, high in the channels and low in the surrounding particle structures, cannot be resolved.

In Fig. 2e the outcome for 4 mm x 4 mm x 11 mm elongated cuboids is given. Experiment and simulation are in good agreement for the entire velocity range with average deviations of $\overline{\Delta p} = 20\ Pa$. Deviations between two runs of the same experiment are small with an average deviation of $\overline{\Delta p} = 23\ Pa$.

4.2 Particle orientation analysis

As the particle orientation plays an important role for the fluidization behavior and process quality of fluidized beds, the simulations are compared with experiments. Therefore, a Matlab script was written to determine the particle orientations in the experiments based on recorded images. Particle orientations in the simulations are readily available for comparison. To gain statistically relevant data between 50,000 to 250,000 particles have been detected and analyzed per fluid velocity in both DEM-CFD and experiments. Only particles visible through the x-z plane have been analyzed in the simulations to achieve equal conditions for both cases. Particle orientation distributions for four different particle shapes, excluding the spheres, are given in Fig. 3 with numerical results in the left and experimental results being shown in the right column. The error bars in Fig. 3 show the uncertainty of the developed script which is gained from the comparison with manually analyzed samples. As the numerical results have been analyzed based on the calculated data and are therefore exact, no error bars are shown in the left column of Fig. 3.

Orientations for 4 mm x 14 mm elongated cylinders are given in in Fig. 3a and Fig. 3b in the range from -89° to 90° of the x-z plane. As -90° and 90° express identical orientations and cannot be distinguished, all affected particles were classified as 90°. An orientation of 0° represents a particle of which the main axis is horizontal to the x-y plane, while values around -89° and 90° represent a particle with its main axis vertical to the x-y plane. The fixed bed shows deviations for the angles that indicate vertical alignment; these are the predominantly occurring orientations in the experiments, but the least occurring in the simulations.

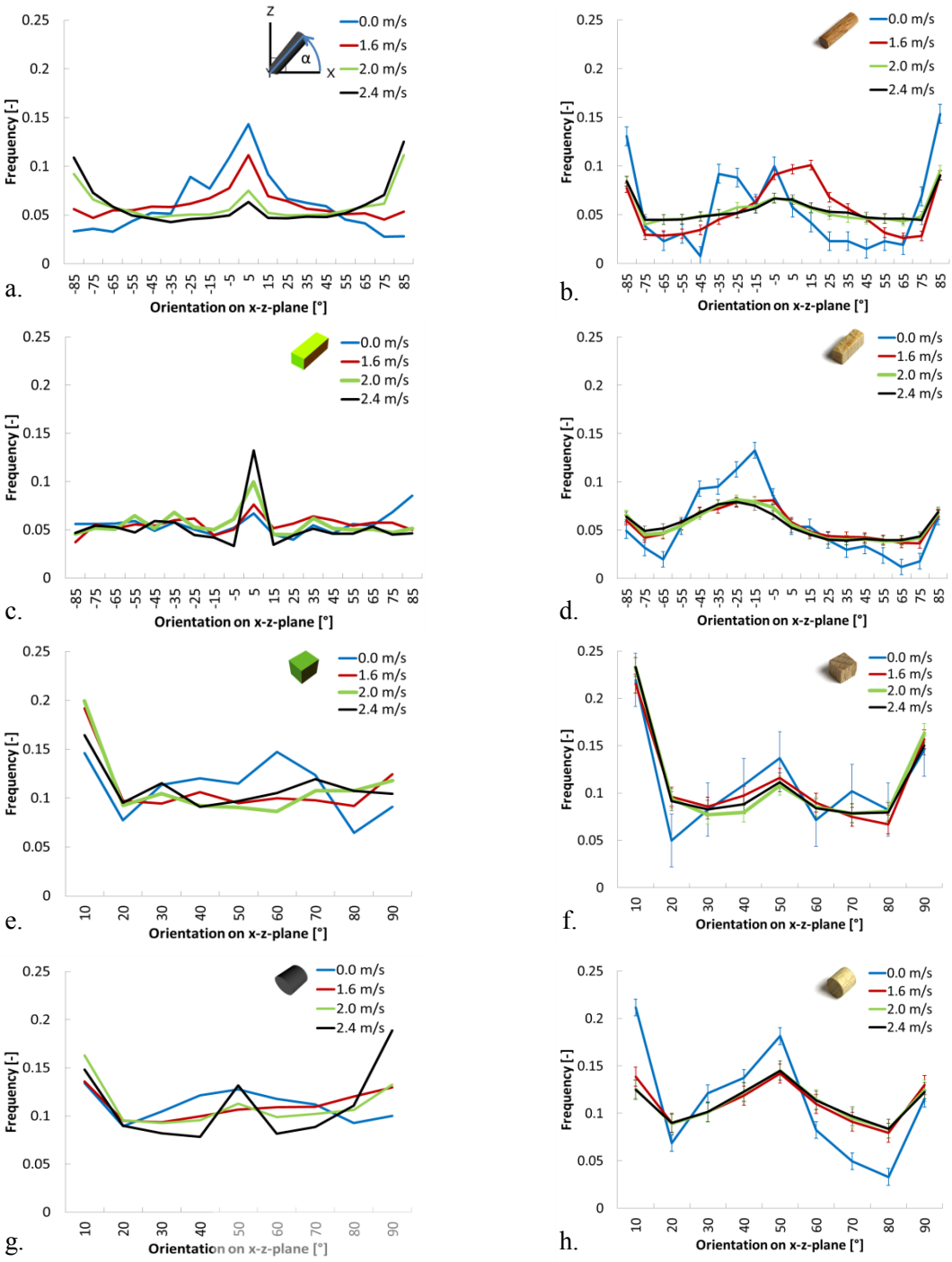

Fig. 3 Frequency distribution of the orientation projected onto the x-z plane for simulations (left column) and experiments (right column) for (a,b) 4 mm x 14 mm elongated cylinders, (c,d) 4 mm x 4 mm x 11 mm elongated cuboids, (e,f) 5 mm x 6 mm x 6 mm cubes and (g,h) 6 mm x 6 mm ideal cylinders

These deviations can explain the differences in the pressure drop of the fixed bed velocity range, which occur despite the comparable bed heights and thereby porosities. With an increase of the superficial velocity the experimental and numerical results fit increasingly

better to each other. Both, simulation and experiment, show that increasing amounts of particles orientate themselves vertically with rising superficial velocities. This finding confirms results indicated in literature [11, 12]. The outcome for 4 mm x 4 mm x 11 mm elongated cuboids is given in Fig. 3c for the DEM-CFD and Fig. 3d for the experiments. For the fixed bed some deviations can be observed between simulation and experiment, this reflects the deviations found in the pressure drop of the fixed bed of the elongated cuboids displayed in Fig. 2e. In the fluidized state the experimental results show only small variations between the three analyzed velocities. The simulations show an increase of horizontally orientated particles with higher velocities, which is the result of particle attachment to the walls as the particles stack up mostly horizontally. Contrary to the 4 mm x 14 mm elongated cylinders, the elongated cuboids do not show an increase of the frequency of the vertical orientations around -89° and 90° with increasing superficial velocities. This confirms the proposition of Cai et al. [11], that particles below a certain elongation ratio behave comparable to equidimensional particles. The DEM-CFD is able to reproduce this behavior. Cuboids with the dimensions 5 mm x 6 mm x 6 mm are displayed in Fig. 3e and Fig. 3f. As the orientation detection is more difficult for equidimensional particles, they are given in the range from 0-90°. The edge of the cube that lies in the range of 0-90° is hereby considered in the analysis. Generally simulation and experiment are in good agreement; both distribution functions remain mostly unchanged for increasing superficial velocities. In Fig. 3g and Fig. 3h the results for the orientations distributions of 6 mm x 6 mm ideal cylinders are displayed. Variations between simulations with different superficial velocities are quite small, and with increasing superficial velocity the orientations become more evenly distributed. Similarly the experimental data shows only small deviations between different superficial fluid velocities.

5 CONCLUSIONS

Pressure drops of 5 differently shaped Geldart-D particle groups have been examined in a laboratory scale fluidized bed, both experimentally and numerically. A combined DEM-CFD approach which considers particle shapes and orientations in the drag force models was used in the simulations. The analysis of the pressure drops showed that DEM-CFD simulations are a useful tool in the description of fluidized systems as the results are in good agreement with the corresponding experiments for most particle types. Minimum fluidization velocities were accurately described by the DEM-CFD except for elongated cylinders which differ strongly from a spherical shape. Particles that differ strongly from a spherical shape show the tendency to form channels for small superficial fluid velocities once the minimum fluidization velocity is passed. These channels result in a lower overall pressure drop as not all particles are fully suspended. The DEM-CFD cannot describe this behavior as the flow is not fully resolved around the particles but only calculated as a cell averaged value. The analysis of the particle orientation showed that differences in the pressure drop of fixed beds at equal bed heights and therefore porosities can be explained through differences in the orientation distributions between experiments and simulations. It was found that elongated cylinders show a tendency to align themselves with the flow with increasing superficial velocities, which confirms findings from the literature [11, 12].

ACKNOWLEDGEMENTS

The financial support by the DFG - KR 3446/6-1 is greatly acknowledged.

REFERENCES

1. Di Felice, R.: *The voidage function for fluid-particle interaction systems*. Int. J. Multiph. Flow. 20, 153–159 (1994).
2. Hölzer, A., Sommerfeld, M.: *New simple correlation formula for the drag coefficient of non-spherical particles*. Powder Technol. 184, 361–365 (2008).
3. Hilton, J.E., Mason, L.R., Cleary, P.W.: *Dynamics of gas–solid fluidised beds with non-spherical particle geometry*. Chem. Eng. Sci. 65, 1584–1596 (2010).
4. Zhou, Z.Y., Pinson, D., Zou, R.P., Yu, a. B.: *Discrete particle simulation of gas fluidization of ellipsoidal particles*. Chem. Eng. Sci. 66, 6128–6145 (2011).
5. Oschmann, T., Hold, J., Kruggel-Emden, H.: *Numerical investigation of mixing and orientation of non-spherical particles in a model type fluidized bed*. Powder Technol. 258, 304–323 (2014).
6. Kruggel-Emden, H., Simsek, E., Rickelt, S., Wirtz, S., Scherer, V.: *Review and extension of normal force models for the Discrete Element Method*. Powder Technol. 171, 157–173 (2007).
7. Kruggel-Emden, H., Wirtz, S., Scherer, V.: *An analytical solution of different configurations of the linear viscoelastic normal and frictional-elastic tangential contact model*. Chem. Eng. Sci. 62, 6914–6926 (2007).
8. Höhner, D., Wirtz, S., Kruggel-Emden, H., Scherer, V.: *Comparison of the multi-sphere and polyhedral approach to simulate non-spherical particles within the discrete element method: Influence on temporal force evolution for multiple contacts.* Powder Technol. 208, 643–656 (2011).
9. Höhner, D., Wirtz, S., Scherer, V.: *Experimental and numerical investigation on the influence of particle shape and shape approximation on hopper discharge using the discrete element method.* Powder Technol. 235, 614–627 (2013).
10. Hold, J.: *Charakterisierung der Mischungs- und Segregationsvorgänge in Modellwirbelschichten mit mono- und bidispersen sphärischen Partikelsystemen : Experimente und gekoppelte CFD / DEM-Modellierung.* , PhD-thesis, Bochum (2013).
11. Cai, J., Li, Q., Yuan, Z.: *Orientation of cylindrical particles in gas-solid circulating fluidized bed.* Particuology. 10, 89–96 (2012).
12. Ku, L.: *Motion and orientation of cylindrical and cubic particles in pipe flow.* J. Zhejian Univ. Sci. 9, 664–671 (2008).